TITLE

Circulating H3K27 Methylated Nucleosome plasma concentration: a synergic information with ctDNA Molecular Profiling

AUTHORS INFORMATION

Emmanuel GROLLEAU [1,2,†], Julie CANDIRACCI [3,†], Gaelle LESCUYER [1,4,5,6], David BARTHELEMY [1,4,5,6], Nazim BENZERDJEB [1,7], Christine HAON [1,5,6], Florence GEIGUER [1,4,5,6], Margaux RAFFIN [1,4,5,6], Nathalie HARDAT [3], Julie BALANDIER [1,4,5,6], Rémi RABEUF [3], Lara CHALABREYSSE [7], Anne-Sophie WOZNY [5,6,8], Guillaume ROMMELAERE [3], Claire RODRIGUEZ-LAFRASSE [5,6,8], Fabien SUBTIL [9], Sébastien COURAUD [1,2], Marielle HERZOG [3], Lea PAYEN-GAY [1,4,5,6,*]

[1] Center for Innovation in Cancerology of Lyon (CICLY) EA 3738, Faculty of Medicine and Maieutic Lyon Sud, Claude Bernard University Lyon I, 69921 Oullins, France.

[2] Pulmonology Department, Lyon Sud Hospital, Hospices Civils de Lyon, 69495 Pierre-Bénite, France.

[3] Belgian Volition SRL, Parc Scientifique Créalys; 5032 Isnes, Belgium.

[4] Institut of Pharmaceutical and Biological Sciences (ISPB), Claude Bernard Lyon I, 69373 Lyon, France.

[5] Department of Biochemistry and Molecular Biology, Lyon-Sud Hospital, Hospices Civils de Lyon, 69495 Pierre-Bénite, France.

[6] Circulating Cancer (CIRCAN) Program, Hospices Civils de Lyon, Cancer Institute, 69495 Pierre-Bénite, France.

[7] University of Lyon, Claude Bernard University, pathology department, Hospices Civils de Lyon; Pierre-Bénite, France.

[8] Cellular and Molecular Radiobiology Laboratory UMR CNRS5822/IP2I, Faculty of Medicine and Maieutic Lyon Sud, Claude Bernard University Lyon I, 69921 Oullins, France.

[9] University of Lyon, Claude Bernard University, statistic department, Hospices Civils de Lyon; Pierre-Bénite, France.

[†] Emmanuel Grolleau and Julie Candiracci have contributed equally to this work

* Correspondence: Léa Payen-Gay, lea.payen-gay@chu-lyon.fr

ABSTRACT

Background: Molecular profiling of circulating tumor DNA (ctDNA) is a helpful tool for cancer treatment indication or for the early detection of relapse. In patients with advanced lung adenocarcinoma cancers (NSCLC), a subset can be cured by immunotherapy, radiotherapy, and/or chemotherapy combined regimens, or targeted therapies depending on their ctDNA molecular profile. But clinical interpretation of ctDNA negative result remains often challenging. Taking advantage that cell-free DNA in association with nucleosomes are released into the bloodstream upon cell death, the characterization of both may give a benefit to patient management. Indeed, dysregulations of epigenetic modifications, such as histone methylation, are found to play a key role in tumorigenesis of different cancers. However, the concentration of circulating nucleosomes in blood, as a biomarker of the contributive value of ctDNA molecular profiling in patient management at diagnosis or during patient follow-up have not previously been investigated.

Results: Significantly elevated concentrations of H3K27Me3-nucleosomes were found in NSCLC plasmas at diagnosis and during the follow-up of patients compared to healthy donors (median: 24ng/mL; 16.9ng/mL vs 8ng/mL, p-value < 0.0001, respectively). Interestingly, by combining H3K27Me3 level and ctDNA molecular profile, we found that 25.5% of the patients

had high levels of H3K27Me3 (above 22.5 ng/mL) and no somatic alteration detected at diagnosis. This strongly supports the presence of non-mutated ctDNA in the corresponding plasma. During patient follow-up, H3K27Me3 level was lower in ctDNA-negative group compared to ctDNA-positive group ($median_{ctDNA-}$ = 13.4 ng/mL vs $median_{ctDNA+}$ = 26.1 ng/mL, respectively, p-value < 0.0001). In 41.8% of the samples, no somatic mutation and low level of H3K27Me3-nucleosomes were observed suggesting molecular indicator of treatment response. In contrast, high H3K27Me3-nucleosome levels were found in 15.1% of the samples despite no somatic mutations being detected allowing the identification of disease progression from 43.1% to 58.2% over molecular profiling only.

Conclusion: H3K27Me3-nucleosome level is proposed to be a useful biomarker of the contributive value of ctDNA molecular profiling at diagnosis by greatly improving the confidence in the negative molecular result in cfDNA in lung cancer. In addition, H3K27Me3-nucleosome could be a promising biomarker for Molecular Residual Disease monitoring in NSCLC during or after treatment.

Keywords

NSCLC, epigenetics, histone PTM, H3K27Me3-nucleosome, ctDNA, liquid biopsy, biomarkers, MRD

BACKGROUND

Nucleosomes are small fragments of chromosomes released into the blood during cell death and consist of a histone octamer core with DNA wrapped around it. Interestingly, the size distribution of the DNA released into circulation (cell free DNA (cfDNA)) corresponds to nucleosomes (≈ 147bp) or chromatosome (nucleosome + DNA linker; ≈ 167bp) (1). CfDNA released into the blood following cell death exists in nucleosomal structures and encapsulated

76 in extracellular vesicles which protects them from degradation rather as free DNA fragments
77 (2, 3, 4, 5). In patients with cancer, cfDNA/nucleosomes are released from tumor cells and may
78 harbor tumor DNA (ctDNA) and a variety of histone of post-translational modifications (PTMs)
79 (6, 7).
80 Histone proteins PTMs such as methylation, acetylation, phosphorylation or citrullination
81 regulate most of DNA-templated processes, including replication, transcription and repair.
82 They function as platforms for the recruitment of specific effector proteins, such as
83 transcriptional regulators or chromatin remodelers (8). They can also change the chromatin
84 structure by disrupting the electrical charges in the histone residues and thus modulate
85 accessibility to the DNA (9, 10). Histone methylation is dynamically controlled by various
86 lysine histone demethylase (HDM) and histone methyltransferase (HMT) enzymes that remove
87 or add the methyl group(s) from the lysine residues. Mis-regulation of the HDM and HMT leads
88 to aberrant levels of histone methylation and have been associated with a variety of cancer types
89 including breast, prostate, lung and brain cancers (11). For example, the HMT enzyme,
90 Enhancer of Zeste Homolog (EZH2), the catalytic subunit of polycomb repressive complex 2
91 (PRC2), responsible for the trimethylation of histone H3 at lysine 27 (H3K27Me3), has been
92 reported to be up regulated in cancer (12, 13). Its overexpression also correlates with breast
93 cancer aggressiveness and poor prognosis (14). In parallel, H3K27Me3 levels are associated
94 with transcriptional repression and have been reported to play an important role in the
95 development and progression of several cancers including lung cancer (15, 16, 17). EZH2-
96 catalyzed H3K27Me3 is also a master regulator of epithelial mesenchymal transition (EMT),
97 an early cellular reprogramming event to facilitate the initial steps of the metastatic cascade
98 (18, 19, 20). EZH2 levels are impaired in tumor angiogenesis and associated with drug
99 resistance phenotype in multiple cancers (21, 22).

100 Epidermal growth factor receptor (EGFR)-tyrosine kinase inhibitors (TKI), such as Osimertinib
101 and Gefitinib, have only been proven to be beneficial for patients with EGFR sensitizing genetic
102 alterations in lung cancer (23). Recently, it had been shown that EZH2 inhibitors could sensitize
103 *in vitro* EGFR wild-type cells to Gefitinib (24). EZH2 is highly expressed in Non-Small Cell
104 Lung Cancer (NSCLC) and is associated with poor prognosis in patients with lung
105 adenocarcinoma. Therefore, targeting H3K27Me3 via EZH2 is a promising cancer therapy.
106 Tazemestostat, is the only EZH2 inhibitor approved by FDA for adults and pediatric patients
107 aged 16 years and older. Currently, there are several ongoing clinical trials for drugs targeting
108 EZH2 in different cancer types (25).
109 Combined ctDNA molecular testing to analyze circulating nucleosomes and their histone PTMs
110 before and after patient's treatment could provide a wider view of the genetic and the epigenetic
111 landscape of a tumor and response to treatment. This would also enable minimal residual
112 disease (MRD) assessment. Therefore, we conducted this retrospective, non-interventional
113 study to i) to determine, at diagnosis, the level of circulating nucleosomes containing
114 methylated histone residues, especially H3K27Me3-nucleosomes as potential biomarkers in
115 patients with stage IV NSCLC; ii) to assess, during treatment, the dynamic levels of
116 H3K27Me3-nucleosomes in NSCLC with different mutated ctDNA status to evaluate MRD to
117 drive the choice of the following treatment line. We studied the ctDNA analysis association
118 with nucleosome biomarkers in two independent cohorts of NSCLC patients: a first one at
119 diagnosis before any treatment, a second one undergoing treatment including chemotherapy,
120 combined or not with immunotherapy, or targeted therapy. Nucleosome measurements were
121 performed on the same sample as the molecular ctDNA testing on the routine setting. This
122 strengthens the accuracy of using biomarkers in patient management of NSCLC.
123 For the first time, we report a high level of circulating H3K27Me3-nucleosomes in NSCLC
124 samples compared to healthy samples and the potential benefit of the combination of

information generated by the measurement of H3K27Me3-nucleosome levels in association with the molecular ctDNA profile at diagnosis for the patient management. We also highlight the putative role of circulating H3K27Me3-nucleosomes as blood-based biomarkers for quantifying the MRD to monitor NSCLC patients during treatment.

RESULTS

High levels of circulating H3K27Me3-nucleosomes are observed in NSCLC samples at diagnosis

The concentration of circulating nucleosomes with specific methylated marks H3K27Me3-, H3K36Me3-, H3K9Me3- and H3K4Me2- were measured using chemiluminescent Nu.Q® immunoassays in NSCLC samples (training set (T) $n_T = 203$; validation set (V) $n_V = 116$) and compared to healthy samples ($n_T = 100$; $n_V = 101$). In both sets, we observed significantly higher circulating H3K27Me3-, H3K36Me3- or H3K9Me3-nucleosome levels in NSCLC samples compared to healthy ($median_T$: 22.7 ng/mL *vs* 6.1 ng/mL; 21.8 ng/mL *vs* 11.8 ng/mL; 15.2 ng/mL *vs* 5.7 ng/mL, respectively; p-value < 0.0001 for each and $median_V$: 28.3 ng/mL vs 9.6 ng/mL; 24.0 ng/mL vs 10.0 ng/mL; 20.4 ng/mL vs 7.5 ng/mL, respectively; p-value < 0.0001 for each) (Fig. 1A, B). A lower difference was observed for H3K4Me2-nucleosome levels between NSCLC and healthy samples ($median_T$: 11.3 ng/mL *vs* 10.6 ng/mL and $median_V$ = 12.4 ng/mL *vs* 11.2 ng/mL, respectively; p-value < 0.01 for each), with a very small magnitude (Table S1). The highest change observed between the medians of tumor and healthy samples was observed for the level of H3K27Me3-nucleosomes with a fold change of 3.7 and 2.9 in training and validation sets, respectively (Table S1). This marker also showed the best area under the ROC (receiving operating characteristics) curve (AUC) with a value of 0.92 (95% CI: 0.89 - 0.95) and 0.88 (95% CI: 0.84 - 0.93) corresponding to the training and validation sets analysis (Fig. 1C, D and Fig. S1A, B). The sensitivity of the H3K27Me3 assay reached 69.5%

150 (95% CI: 61.8% - 74.5%) at 95% specificity in the training set. These clinical performances
151 were confirmed in the validation set where the sensitivity reached 68.7% (95% IC: 59.7% -
152 76.5%%) at 95% specificity (Fig. 1C, D and Table S2A, B).
153

154 **H3K27Me3-nucleosome levels correlate with cfDNA quantity and percentage of**
155 **Mutational Allele Fraction (MAF) at diagnosis**

156 Circulating nucleosomes containing the methylated histone marks and quantity of cfDNA or
157 the percentage of mutated allele MAF correlated well (Fig. 2). The training and validation sets
158 were combined into one whole cohort to increase the number of samples per group for better
159 accuracy (n_{NSCLC} = 319; $n_{HEALTHY}$ = 201). At diagnosis, patients with NSCLC showed a strong
160 positive correlation between the levels of cfDNA and H3K27Me3-,H3K36Me3-, or H3K9Me3-
161 nucleosome (r = 0.78; 0.66 and 0.75, respectively, p-value < 0.0001) and a moderate correlation
162 with H3K4Me2-nucleosome (r = 0.53; p-value < 0.0001). The percentage of MAF for genomic
163 somatic alterations in plasma samples was defined using the ratio absolute count of read
164 between the reference and mutated forms. All H3K27Me3-, H3K36Me3-, H3K9Me3-
165 ,H3K4Me2-nucleosome levels and cfDNA concentration showed a weak, but statistically
166 highly significant correlation coefficient with the percentage of MAF (r = 0.33; 0.31; 0.32 and
167 0.21, respectively; p-value < 0.0001 and r = 0.28; p-value < 0.001, respectively) (Fig. 2).
168

169 **H3K27Me3 expression level in normal and adenocarcinoma tissue.**

170 The immunohistochemical investigation of tissue microarrays (TMAs) of normal pneumocytes
171 (n = 18) showed moderate to high H3K27Me3 expression level in 83% of cases (Fig. 3A). In
172 the alveolar region (parenchyma) of normal lung tissue, where air and blood are brought in
173 closed proximity over a large surface, the barrier between air and blood consists of a continuous
174 alveolar epithelium (a mosaic of type I and type II alveolar epithelial cells), a continuous

175 capillary endothelium and the connective tissue layer in-between, as showed in Fig. 3A. In
176 contrast in tumoral tissue (n = 50, two cores per patient), remodeling structural events occurred
177 (Fig. 3B, C, D). We observed i) weak H3K27Me3 expression level in 42% of cases (Fig. 3B),
178 ii) moderate expression level in 37% of cases (Fig. 3C), and iii) high expression level in 21%
179 of cases (Fig. 3D). TMAs of lung adenocarcinoma showed heterogeneous H3K27Me3
180 expression levels within the same patient demonstrating an intra-tumoral heterogeneity (data
181 not shown). The analysis of H3K27Me3 expression as a function of grade showed that the
182 expression of H3K27Me3 is associated with the tumor grade. Higher H3K27Me3 expression
183 was observed in tumor grades 2 and 3 (Fig. 3E). In contrast, H3K27Me3 expression
184 heterogeneity was not associated with the tumor grade.
185

186 **Relevant combined information from circulating H3K27Me3-nucleosome levels and**
187 **ctDNA molecular profile at diagnosis**

188 As H3K27Me3-nucleosome level is high in NSCLC samples but showed a low, although
189 significant correlation, with MAF; we asked if H3K27Me3 levels could bring additional
190 information relative to the potential presence of circulating tumor material or process. To
191 address this question, we first defined the upper limit of the reference interval of H3K27Me3-
192 nucleosomes in a healthy population. As the distribution of the training and validation sets were
193 similar (Fig. S2), we combined the two sets of samples into a global and homogenous healthy
194 cohort (n = 201) in which no outlier was identified using both the D/R ratio and ROUT methods.
195 The upper limit of the reference interval including 95% of this population was calculated at
196 18.4 ng/mL (SD = 4.07). Then, we defined a cut-off at 22.5 ng/mL (18.4+1SD) ensuring 100%
197 specificity in both training and validation sets. In the whole NSCLC cohort (n = 318), 53.1%
198 of the patients (n = 169) showed H3K27Me3-nucleosome levels above the cut-off (Fig. 4A).
199 The presence or absence of somatic alterations was reported on the same plasma samples based
200 on DNAseq next-generation sequencing (NGS) analysis (the comprehensive panel contains the

201 major 78 oncodrivers known in NSCLC). In the whole NSCLC cohort, there were 41.2%
202 samples for which at least one somatic alteration or copy number variation (CNV) was
203 identified, referred to hereafter as ctDNA positive sample (ctDNA+; n = 131) and 58.8% of
204 patients for whom no genetic somatic alteration was found and defined as ctDNA negative
205 (ctDNA-; n = 187) hereafter. The level of H3K27Me3-nucleosomes is significantly higher in
206 ctDNA+ group compared to ctDNA- group (median = 33.9 ng/mL vs 18.5 ng/mL; *p*-value <
207 0.001) and compared to healthy group (median = 33.9 ng/mL vs 8.0 ng/mL; *p*-value < 0.0001)
208 (Fig. 4B). H3K27Me3-nucleosome levels were also higher in the ctDNA- group compared to
209 healthy group (median = 18.5 ng/mL vs 8.0 ng/mL; *p*-value < 0.0001).
210 Based on these observations, we compared the tumor mutation burden defined by the ctDNA
211 status of the samples and the H3K27Me3-nucleosome concentrations in a decision tree model
212 (Fig. 5). We sub-classified the samples based on their ctDNA status (ctDNA- or ctDNA+) and
213 based on their H3K27Me3-nucleosome levels defined as H3K27Me3 positive (H3K27Me3+)
214 or H3K27Me3 negative (H3K27Me3-) depending on whether H3K27Me3-nucleosome levels
215 were above or below the defined cut-off at 22.5 ng/mL. We observed that: i) 33.3% of samples
216 were double negative for ctDNA and H3K27Me3; ii) 25.5% of samples were negative for
217 somatic alteration but had a high level of H3K27Me3-nucleosomes; iii) 13.5% samples had a
218 low level of H3K27Me3, even if somatic alterations had been detected; iv) 27.7 % samples
219 were found to be positive for both ctDNA and H3K27me3-nucleosomes (Fig. 5).
220

221 **High level of circulating H3K27Me3-nucleosomes observed in NSCLC samples during**
222 **treatment is more pronounced in presence of mutated ctDNA.**

223 Based on the results observed at diagnosis, we decided to focus our analysis of NSCLC samples
224 collected during patient treatment on H3K27Me3 only to evaluate its level change across the
225 treatment. We assessed the concentration of circulating H3K27Me3-nucleosomes in NSCLC

226 samples (n = 304) in routine settings and compared to healthy samples (n = 201). A highly
227 significant increase was observed in NSCLC compared to healthy samples (median = 16.9
228 ng/mL vs. 8 ng/mL, respectively; *p*-value < 0.0001) (Fig. 6A). In this NSCLC population, the
229 H3K27Me3-nucleosome levels were lower than samples collected at diagnosis ($median_{DURING}$
230 $_{TREATMENT}$ = 16.9 ng/mL vs $median_{AT\ DIAGNOSIS}$ = 24 ng/mL *p*-value < 0.0001).
231 The molecular profiles of these NSCLC samples were conducted by NGS analyses. In 43.1%
232 of the samples (n =131), at least one mutation among the 78 screened genes was detected,
233 demonstrating the presence of ctDNA in plasma samples. Then, we compared the circulating
234 H3K27Me3-nucleosome levels in positive and negative ctDNA samples (ctDNA+, ctDNA-)
235 collected during the treatment. The level of circulating H3K27Me3-nucleosomes was lower in
236 the ctDNA-negative group compared to ctDNA-positive group ($median_{ctDNA-}$ = 13.4 ng/mL vs
237 $median_{ctDNA+}$ = 26.1 ng/mL, respectively, *p*-value < 0.0001) (Fig. 6B). A greater heterogeneity
238 of H3K27Me3-nucleosome levels was observed in presence of somatic alteration, 55% of
239 samples were found above the H3K27Me3-nucleosomes cut-off in the ctDNA+ group, whereas
240 only 26.6% of the samples were above in the ctDNA- group (Fig. 6B). The clinical performance
241 was then evaluated on the whole cohort (in grey), on the ctDNA- (dotted line) and ctDNA+ (in
242 black) sub-groups in comparison to the healthy samples (Fig. 6C, Table S3). We found that the
243 discrimination of NSCLC samples was improved in ctDNA+ sub-group with an AUC of 0.87
244 compared to 0.74 for ctDNA- sub-group and 0.79 for the whole cohort respectively; *p*-value <
245 0.0001) (Fig. 6C, D).
246
247 **Additive value of both biomarkers: H3K27Me3-nucleosomes and ctDNA**
248 After sub-grouping of NSCLC samples collected during treatment into ctDNA- and ctDNA+
249 classification; samples were further classified based on their level of circulating H3K27Me3-
250 nucleosomes below or above the cut-off at 22.5 ng/mL, as H3K27Me3-negative (H3K27Me3-

251) or H3K27Me3-positive (H3K27Me3+) and organized in four classes described in a decision
252 tree (Fig. 7A). We observed i) 41.8% of samples are double negative for the ctDNA and
253 circulating H3K27Me3-nucleosome levels (ctDNA- H3K27Me3-); ii) 15.1% of samples are
254 negative for somatic alteration but positive for circulating H3K27Me3-nucleosomes (ctDNA-
255 H3K27Me3+); iii) 19.4% of samples had a level of circulating H3K27Me3-nucleosomes below
256 22.5 ng/mL, even when somatic alterations had been detected (ctDNA+ H3K27Me3-); iv)
257 23.7% of samples were found to be positive for both ctDNA and circulating H3K27Me3-
258 nucleosome levels (ctDNA+ H3K27Me3+).
259
260 **High circulating H3K27Me3-nucleosome levels are preferentially associated with TP53**
261 **mutations during treatment.**
262 In ctDNA+ group, levels of circulating H3K27Me3-nucleosomes were compared based on the
263 mutation status of three major oncodrivers of interest: EGFR, KRAS and TP53. Mutational
264 status in the corresponding sub-groups was annotated as positive (+) when at least one mutation
265 was detected and negative (-) when no mutation was detected (Fig 7). In parallel of the tendency
266 of association found at diagnosis (data not shown), significant increase of circulating
267 H3K27Me3-nucleosome levels was observed in TP53+ (n = 72) sub-group compared to TP53-
268 (n = 59) sub-group ($median_{TP53+}$ = 36.9 ng/mL vs $median_{TP53-}$ = 19.2 ng/mL; *p*-value < 0.05) (Fig.
269 8 A-B). No difference was observed in comparisons between EGFR+ versus EGFR- neither
270 KRAS+ versus KRAS- sub-groups ($median_{EGFR+}$ = 21.8 ng/mL vs $median_{EGFR-}$ = 36.3 ng/mL; *p*-
271 value = 0.22; $median_{KRAS+}$ = 14.8 ng/mL vs $median_{KRAS-}$ = 26.7 ng/mL; *p*-value = 0.50) (Fig. 8
272 A-B).
273
274 **DISCUSSION**

275 Patient management with NSCLC is based on histopathological evaluation completed with
276 protein and molecular biomarkers for determining the optimal treatment. Tumor tissue-based
277 molecular testing has demonstrated its utility to assess patients for the recommended
278 biomarkers but remains challenging due to tissue invasive sampling, DNA quantity availability
279 and heterogeneity, and inadequacy of repeated testing (26). In contrast, genomic somatic testing
280 of oncodrivers through liquid biopsy has emerged as a key strategy for managing patients that
281 are diagnosed with an advanced NSCLC and can be used both at diagnosis to define first-line
282 therapy and throughout patient follow-up to identify the emergence of resistant mechanisms.
283 Therefore, although tissue biopsy remains the reference standard for cancer diagnosis and
284 patient management, when combined with plasma-based molecular profiling, the patient
285 standard of care is improved by approximately 11 to 20% (27, 28, 29). In contrast to tissue
286 biopsies, plasma testing can be easily repeated serially to monitor response and may allow
287 detection of minimal residual disease prior to ct-scan or clinical progression. It also reduces
288 invasiveness and costs. In consequence, it is more compliant for patients. Despite the high
289 clinical specificity of ctDNA, physicians often face a high non-contributive detection rate of
290 preoperative mutated plasma ctDNA, around 24% to 85% in the overall population of lung
291 cancers associated with stage in routine settings (30, 31, 32). CtDNA was detected after
292 treatment in 64.3% of patients who had obvious clinical recurrence (33). Moreover, a study
293 conducted by Chaudhuri et al., showed that disease recurrence in ctDNA negative population
294 happened in 6% of the post-operative population of NSCLC patients (34). So currently, the
295 interpretation of an undetectable ctDNA is still a significant limitation in clinical indication.
296 Other circulating biomarkers may complement ctDNA molecular testing. Circulating
297 nucleosome as the carrier of genetic and epigenetic information and genetic aberrations could
298 be one of these. In addition, thanks to the low volumes required for the nucleosome Nu.Q®
299 immunoassay, it is easy to add it at the plasma molecular profiling testing on the same plasma

300 sample. In this study, we focused on circulating H3K27Me3-nucleosome levels in NSCLC
301 patients at diagnosis or during their treatment, and the combined contributive information to
302 molecular profiling of circulating H3K27Me3-nucleosomes.
303
304 TMA analysis showed that H3K27Me3 was detected in the nucleus of normal adjacent cells
305 and adenocarcinoma cells. Histone modification is a dynamic process as demonstrated recently
306 by FRET (fluorescence resonance energy transfer) biosensor-based technique in cancer living
307 cells (35). Unlike H3K9Me3 that is always associated with silenced chromatin regions,
308 H3K27Me3 mark is found in bivalent domains associated with gene repression but still allow
309 these genes to be activated (36). The repression was not randomly distributed within the genome
310 but enriched in inactive topologically associated domains (TADs) with low expression of genes
311 involved in proliferation (37, 38). As described for genetic clonality profiling and PD-L1
312 (programmed death ligand 1) tissue expression, we observed intra- and inter-tumoral
313 heterogeneity in adenocarcinomas (39). Interestingly, the frequency of high expression of
314 H3K27Me3 was larger in grade 3 adenocarcinoma compared to grade 2 and grade 1 suggesting
315 that in NSCLC, like in thyroid cancer or invasive phenotype of melanoma, H3K27Me3
316 overexpression could be positively associated with tumor aggressiveness (40, 41). Cellular
317 plasticity and tumor cells dedifferentiation is commonly observed in various types of
318 malignancies and is described to be associated with increased tumor cell invasiveness and drug
319 resistance. We can speculate that the association between H3K27Me3 level and tumor
320 aggressiveness could be linked with its role in this loss of differentiation of tumor cells (42, 43,
321 44). At diagnosis, circulating H3K27Me3-nucleosome levels are significantly higher in NSCLC
322 patients compared to healthy donors. In contrast to tissue observation, this analysis of
323 circulating H3K27Me3-nucleosomes reflects the release of nucleosomes into the blood
324 following cell death and high cell turnover occurring in cancer (45, 46, 47).

325 To discuss the advantage of the quantification of H3K27Me3-nucleosomes in clinical settings,
326 we had to establish the normality range into healthy population using similar methodology as
327 other tumoral biomarkers such as CYFRA21.1 and CA125. For doing that, we first determined
328 the upper limit of the reference interval of H3K27Me3-nucleosomes in a healthy population
329 and determined the threshold of positivity at 22.5 ng/mL ensuring 100% specificity in both
330 training and validation sets. Increased H3K27Me3-nucleosome levels observed in NSCLC
331 patients was even more pronounced in patients who have somatic alterations and was logically
332 positively associated to the cfDNA concentration as its carrier. Somatic mutations were found
333 in 41.2% of analyzed samples. 27.7% of the samples were positive for both ctDNA and
334 circulating H3K27Me3-nucleosomes pointing to putative epigenetic and mutational burden
335 processes, while in 13.5% samples only somatic alterations were detected demonstrating the
336 presence of tumoral material in blood but a low level of H3K27Me3-nucleosome which might
337 suggest a low-grade tumor or epigenetic changes compared to normal cells as supported by the
338 TMA analysis performed.
339 Besides, one fourth of patients (25.5%) had a high H3K27Me3-nucleosome levels even if no
340 somatic alteration were detected in plasma. This is indicative of tumoral DNA release into blood
341 despite absence of somatic alteration detected, indicating somatic mutation not covered by the
342 comprehensive panel of genes used in the customized NGS assay and potentially a high-grade
343 cancer. We can hypothesize that most likely nucleosome and its associated DNA came from
344 cancer cells but from a genomic region that did not have a cancerous mutation. Those samples
345 could be considered as true ctDNA negative for the main oncodriver alterations. In the opposite,
346 33.3% of the samples were negative for both ctDNA and H3K27Me3-nucleosome level
347 indicating no or very few tumoral material released into blood. In this case, a re-biopsy will be
348 probably required for those patients at diagnosis until additional cancer biomarkers are
349 identified. Altogether, these results at diagnosis showed that by combining circulating

350 H3K27Me3-nucleosome levels with genomic testing, we can increase the contributing
351 information of ctDNA sequencing by 25.5% to help interpret negative ctDNA results. In
352 addition, high level of H3K27Me3-nucleosomes in half of the cases (52%) could be used as a
353 biomarker to monitor patients during follow-up.
354 During patient's treatment, high levels of circulating H3K27Me3-nucleosomes were still
355 observed in NSCLC samples especially in presence of mutated ctDNA. Nevertheless, we can
356 note that despite being still high, the H3K27Me3-nucleosome levels in the ctDNA negative
357 group were closer to the one observed in the healthy group with 61.2% of the samples below
358 the cut-off. As the study was conducted on two independent cohorts at diagnosis and during
359 treatment, it was not possible to make a direct comparison. But Holdenrieder and al. described
360 that in patients with advanced lung cancers, levels of circulating nucleosomes at diagnosis were
361 significantly lower in patients who responded to chemotherapy, suggesting that nucleosome
362 could be a potential predictive biomarker (48). When combining both ctDNA sequencing and
363 H3K27Me3-nucleosome measurements, we observed nearly 42% of the samples negative both
364 ctDNA and H3K27Me3-nucleosomes suggesting no detection of tumoral material and a
365 potential positive evolution of the disease. First-line treatment should be continued, and the
366 next follow-up may be spaced out in time (Fig. 7B). In 15% of the samples, no somatic mutation
367 was found but a high level of circulating H3K27Me3-nucleosomes was detected. This could
368 illustrate a progression of the disease in absence of acquisition of somatic mutation, or no
369 alteration covered by the NGS comprehensive gene panel. A change in the treatment to classic
370 second line therapy may be considered (Fig. 7B). These results could also suggest that a
371 combined therapy with EZH2-inhibitor might be appropriate. More clinical data on EZH2
372 inhibitor performances in NSCLC are required to confirm or not this option. Somatic mutations
373 have been detected in the remaining 43% of the samples associated with a high level of
374 H3K27Me3-nucleosomes (23.7%) or not (19.4%) demonstrating a progression of the cancer

375 and the need to change the treatment (Fig. 7B). Importantly, when the level of H3K27Me3-
376 nucleosomes is considered with ctDNA there was an increased identification of disease
377 progression from 42 to 58% of patients. In addition to the potential benefit to combine
378 H3K27Me3-nucleosomes and ctDNA analysis at diagnosis to ascertain a true negative ctDNA
379 results, we propose that H3K27Me3-nucleosomes could also be a good potential biomarker to
380 detect minimal residual disease and to monitor response during disease progression. Further
381 studies would be required to validate the potential of circulating H3K27Me3-nucleosomes as
382 biomarker for NSCLC patient follow-up. When validated, we could consider implementing the
383 measurement of H3K27Me3-nucleosomes before molecular profiling analysis for an improved
384 patient care and a more cost-efficient health care system. Indeed, if during post-treatment, the
385 patient is well with normal scan images and low H3K27Me3-nucleosomes levels, ctDNA
386 analysis could be postponed. In contrast, high level of H3K27Me3-nucleosomes levels should
387 trigger a quicker ctDNA analysis and therapeutic decision.
388 In French population, the frequency of tissue somatic alterations reported in patient with
389 NSCLC is 11% in *EGFR*, 1% in *HER2*, 29% in *KRAS* 2% in *BRAF*, and 2% *PIK3CA (49)*. In
390 our study, the molecular status was not fully associated with the H3K27Me3-nucleosome
391 concentrations. Nevertheless, the TP53 status, especially during progression, seems to be
392 correlated with the H3K27Me3-nucleosome concentration. 40% TP53 somatic alterations are
393 reported in NSCL (50, 51, 52). This detection is an indicator of a poor prognosis in patients
394 with NSCLC. In advanced NSCLC patients treated with nivolumab, with or without CTLA-4
395 blocker ipilimumab, or pembrolizumab, the median overall survival in the TP53-mutated group
396 was 18.1 months vs 8.1 in the TP53-wild-type group. This strongly indicated that TP53 status
397 might be potential predictor of immunotherapy response (53). These TP53 mutations may differ
398 according to different pathological types and clinical stages and are often detectable during
399 progression or in aggressive grade. These findings agreed with the higher level of H3K27Me3-

400 nucleosome into TP53 mutated samples observed in our cohorts. In this report, the H3K27Me3-
401 nucleosome concentration was not statistically different according to the EGFR and KRAS
402 status and must be addressed in a wider cohort.

403

404 **CONCLUSIONS**

405 Using a simple and low-cost H3K27Me3-nucleosomes immunoassay to complete the molecular
406 exploration of ctDNA could greatly improve confidence in the negative molecular results at
407 diagnosis. This may allow to reduce re-biopsy invasive acts. High levels of H3K27Me3-
408 nucleosomes could allow physicians to detect MRD in NSCLC patients at defined intervals of
409 treatment and recovery to incorporate analysis of evolving molecular landscapes during
410 treatment. These data should be confirmed in a longitudinal study where NSCLC patients will
411 be followed from diagnostics to recovery or relapse.

412

413 **METHODS**

414 **Study Population:**

415 Patients were recruited from the pulmonology department at Lyon University Hospital from
416 2015 to 2022. K2-EDTA plasma heathy samples were provided by the French agency named
417 "Etablissement Français du Sang" (Etude RNIPH 22-5065 NUCLEO_CIRCAN avis CSE n°22-
418 5065). Inclusion criteria were: age over 18 years old with histologically proven NSCLC cancer.
419 For each sample, medical data were collected through a mandatory prescription sheet attached
420 to each sample and edited by the prescribing physician. K2-EDTA plasma samples from 319
421 patients at diagnosis and from 309 independent patients under treatment, defined by a clinical
422 or CT-scan modification during their treatment were analyzed.

423

424 **CfDNA Collection:**

425 Total EDTA blood samples were centrifuged for 10 min at 1600 g. The supernatant was then
426 centrifuged at 6000 g for 10 min, and the resulting plasma was stored at −80 °C until cfDNA
427 extraction and molecular analyses (54). CfDNA was extracted using the QIAamp Circulating
428 Nucleic Acid Kit (Qiagen, Valencia, CA, USA, Cat No 55114), with a Qiagen vacuum manifold
429 following the manufacturers' instructions. CfDNA samples were quantified using a Qubit™ 4
430 Fluorometer (Invitrogen™, Cat No Q33238, Carlsbad CA, 92008, United States) with the
431 Qubit™ dsDNA HS Assay Kit (Invitrogen™, Cat No 32854).
432
433 **Library Preparation for DNA Sequencing:**
434 For custom-validated NGS library preparation, 10 – 100 ng cfDNA were used, using a custom
435 capture-based technology provided by SOPHiA GENECTICS (Lausanne, Switzerland) and
436 performed according to the manufacturer's instructions (55, 56, 57). The custom panel covered
437 78 genes involved in cancer (such as *EGFR*, *TP53* or *KRAS*). The libraries were sequenced on
438 NextSeq 550 (Illumina technology, San Diego, CA 92122) in 2 × 150 paired-end runs. The
439 subsequent Variant Call Files were subjected to cross-sample background filtering, with
440 potential artefacts removed below 3 standard deviations of the mean background noise for each
441 position. -The bioinformatics was performed using the SOPHIA DDM™ platform.
442
443 **Nu.Q® ImmunoAssays:**
444 Four nucleosome structures were measured using Nu.Q® prototype Immunoassays: Nu.Q®
445 H3K27Me3, Nu.Q® H3K36Me3, Nu.Q® H3K9Me3, Nu.Q® H3K4Me2 (Belgian Volition SRL,
446 Isnes, Belgium) according to the manufacturer's instruction. Briefly, these sandwich
447 immunoassays are based on magnetic beads and chemiluminescence technology and are
448 performed on the IDS-i10 automated immunoanalyzer system (Immunodiagnostic Systems Ltd
449 (IDS), UK). 50 µL of K2-EDTA plasma (same as for the DNA sequencing) are incubated with

450 acridinium ester labeled anti-nucleosome antibody. Then, magnetic particle beads, coated with
451 the corresponding monoclonal anti-histone modification capture antibody (i.e., anti-histone
452 H3K27Me3, anti-histone H3K36Me3, anti-histone H3K9Me3, or anti-histone H3K4Me2,
453 respectively), are added. Finally, after a wash step, trigger solutions are added, and the light
454 emitted by the acridinium ester is measured by the luminometer system. The results are
455 expressed in relative light unit (RLU) and the concentrations are extrapolated using a four-
456 parameter logistic regression of a reference standard curve. All samples are analyzed in
457 simplicate.
458
459 **Tissue microarray (TMA):**
460 Two TMAs were purchased from the company TissueArray.com. The first TMA corresponds
461 to 100 cores of 50 cases (2 cores by case) of lung adenocarcinoma (BC04022a), while the
462 second TMA contains 18 cases of squamous cell carcinoma, matched with adjacent normal lung
463 tissue and cancer adjacent tissue per case (LC10014a).
464 The immunohistochemical analysis was performed with an automated immunostainer (BOND).
465 Briefly, formalin-fixed paraffin-embedded 4-µm-thick sections were first19 paraffinized in
466 xylene and rehydrated in ethanol. The endogenous peroxidase activity was blocked (Ventana
467 Medical Systems, Tucson, Arizona, USA) before antigen retrieval was begun. The ULTRA
468 Cell Conditioning Solution (ULTRA CC1) from Ventana Medical Systems was then used for
469 antigen retrieval. Immunohistochemical staining was carried out on an automated
470 immunostainer, with primary antibody. This was followed by application of the avidin–biotin–
471 peroxidase complex technique. Reactions were developed with diamino-3,3′-benzidine
472 tetrahydrochloride substrate solution (SIGMAFAST; Sigma-Aldrich, Tucson, Arizona, USA).
473 The tissues were counterstained with hematoxylin. The primary antibodies and final dilutions
474 were: H3K27Me3 (Cell Signaling Technology, Danvers, Massachusetts, USA).

Immunostaining in the tumor tissue was determined by visual scoring of the brown stain. Scoring of the intensity of the staining was performed according to an arbitrary scale with steps of 0, 1, 2, and 3 where "0" was considered to be absence of staining, "1" considered weak staining, "2" was considered as moderately positive staining, and "3" was considered to be strong staining.

Statistics:

Statistical analyses were performed using GraphPad Prism (GraphPad Prism software version 9.5.0, San Diego, CA, USA). Descriptive statistics were used, and results are reported as mean, median, 2.5th-25th-75th and 97.5th percentiles. Data were subjected to Kolmogorov–Smirnov normality test. As data are not normally distributed, non-parametric methods were used: Mann-Whitney U test and Kruskal-Wallis H test for groups comparison and Spearman's rank correlation for measuring the dependence between variables. Significance values are represented by *: p-value < 0.05; **: $p < 0.01$; ***: $p < 0.001$; ****: $p < 0.0001$. Reference interval (also referred as normal range) of H3K27Me3-nucleosome levels was calculated on global healthy cohort to reach the statistically significant minimum number ($n \leq 120$). The data were subjected to D/R ratio and ROUT methods for the detection of outliers. Reference interval includes 95 % of the population, centred on the median. One standard deviation was added to the upper limit of this reference interval to determine the cut-off.

Study limitations:

As this is a retrospective study carried out for routine use, we are facing limitations, including: i) access to clinical data is limited to ctDNA molecular profile and time of sampling in the routine patient management; ii) we did not have matched tissue-plasma samples, the

499 histological analyses were performed with the commercial Tissue Macro-Array. iii)
500 independent cohorts were analyzed at diagnostic and during treatment.
501
502 **DECLARATIONS**
503 **Ethics approval and consent to participate**
504 Patients were recruited from the pulmonology department at Lyon University Hospital from
505 2015 to 2022 (Etude RNIPH 22-5065 NUCLEO_CIRCAN avis CSE n°22-5065).
506
507 **Consent for publication**
508 Medical data were collected through a mandatory prescription sheet and edited by the
509 prescribing physician. The patients were orally informed of the testing by physicians
510 conducting their clinical management.
511
512 **Availability of data and materials**
513 The data presented in this study are available in the Additional Files and from the
514 corresponding author: lea.payen-gay@chu-lyon.fr
515
516 **Competing interests**
517 J.C., N.H., R.R., G.R. and M.H. are employees of Belgian Volition SRL.
518
519 **Funding**
520 The authors thank AstraZeneca and Belgian Volition for financial support.
521
522 **Authors' contributions**

523 Conceptualization: E.G., D.B., M.H. and L.P.-G.; data curation: J.C., G.L., F.G., J.B. and
524 L.P.-G., formal analysis: E.G., J.C., D.B., M.H. and L.P.-G.; funding acquisition: S.C , and
525 L.P.-G; investigation: C.B., D.B., E.G., A.G., R.R and L.P.-G; methodology: F.S., D.B., G.L.,
526 N.H., M.H. and L.P.-G; project administration: C.R.-L., S.C., M.H. and L.P.-G.; resources:
527 S.C. and E.G.; supervision: M.H. and L.P-G.; validation: all authors; writing—original draft:
528 E.G., J.C., B.B., G.L., D.B., M.H. and L.P.-G; writing-review and editing: J.C., B.B., G.L.,
529 D.B., A.-S.W., S.C., M.H. and L.P.-G. All authors have read and agreed to the published
530 version of the manuscript.
531

532 **Acknowledgements**
533 The authors are very grateful to AstraZeneca for their long-term collaboration with CIRCAN
534 team from Lyon-Sud Hospital. The authors thank AstraZeneca and Sysmex Inostics for their
535 continued financial support of this clinical study. The authors wish thanks the Assay
536 Development team from Belgian Volition for their technical support. We also thank Terry
537 Kelly for critical reading of the manuscript.
538

539 **REFERENCES**

540 1. Fan HC, Blumenfeld YJ, Chitkara U, Hudgins L, Quake SR. Noninvasive diagnosis of fetal
541 aneuploidy by shotgun sequencing DNA from maternal blood. Proc Natl Acad Sci U S A.
542 2008;105(42):16266-71.
543 2. Holdenrieder S, Stieber P, Chan LY, Geiger S, Kremer A, Nagel D, et al. Cell-free DNA in serum
544 and plasma: comparison of ELISA and quantitative PCR. Clin Chem. 2005;51(8):1544-6.
545 3. Wimberger P, Roth C, Pantel K, Kasimir-Bauer S, Kimmig R, Schwarzenbach H. Impact of
546 platinum-based chemotherapy on circulating nucleic acid levels, protease activities in blood and

547 disseminated tumor cells in bone marrow of ovarian cancer patients. Int J Cancer. 2011;128(11):2572-
548 80.
549 4. Heitzer E, Auinger L, Speicher MR. Cell-Free DNA and Apoptosis: How Dead Cells Inform About
550 the Living. Trends Mol Med. 2020;26(5):519-28.
551 5. Fernando MR, Jiang C, Krzyzanowski GD, Ryan WL. New evidence that a large proportion of
552 human blood plasma cell-free DNA is localized in exosomes. PLoS One. 2017;12(8):e0183915.
553 6. Diaz LA, Jr., Bardelli A. Liquid biopsies: genotyping circulating tumor DNA. J Clin Oncol.
554 2014;32(6):579-86.
555 7. Fullgrabe J, Kavanagh E, Joseph B. Histone onco-modifications. Oncogene. 2011;30(31):3391-
556 403.
557 8. Licht JD, Bennett RL. Leveraging epigenetics to enhance the efficacy of immunotherapy. Clin
558 Epigenetics. 2021;13(1):115.
559 9. Fenley AT, Anandakrishnan R, Kidane YH, Onufriev AV. Modulation of nucleosomal DNA
560 accessibility via charge-altering post-translational modifications in histone core. Epigenetics
561 Chromatin. 2018;11(1):11.
562 10. Greer EL, Shi Y. Histone methylation: a dynamic mark in health, disease and inheritance. Nat
563 Rev Genet. 2012;13(5):343-57.
564 11. Zhao Z, Shilatifard A. Epigenetic modifications of histones in cancer. Genome Biol.
565 2019;20(1):245.
566 12. Varambally S, Dhanasekaran SM, Zhou M, Barrette TR, Kumar-Sinha C, Sanda MG, et al. The
567 polycomb group protein EZH2 is involved in progression of prostate cancer. Nature.
568 2002;419(6907):624-9.
569 13. Comet I, Riising EM, Leblanc B, Helin K. Maintaining cell identity: PRC2-mediated regulation of
570 transcription and cancer. Nat Rev Cancer. 2016;16(12):803-10.

571 14. Kleer CG, Cao Q, Varambally S, Shen R, Ota I, Tomlins SA, et al. EZH2 is a marker of aggressive
572 breast cancer and promotes neoplastic transformation of breast epithelial cells. Proc Natl Acad Sci U S
573 A. 2003;100(20):11606-11.
574 15. Wiles ET, Selker EU. H3K27 methylation: a promiscuous repressive chromatin mark. Curr Opin
575 Genet Dev. 2017;43:31-7.
576 16. Wan L, Li X, Shen H, Bai X. Quantitative analysis of EZH2 expression and its correlations with
577 lung cancer patients' clinical pathological characteristics. Clin Transl Oncol. 2013;15(2):132-8.
578 17. Sato T, Kaneda A, Tsuji S, Isagawa T, Yamamoto S, Fujita T, et al. PRC2 overexpression and
579 PRC2-target gene repression relating to poorer prognosis in small cell lung cancer. Sci Rep.
580 2013;3:1911.
581 18. Cardenas H, Zhao J, Vieth E, Nephew KP, Matei D. EZH2 inhibition promotes epithelial-to-
582 mesenchymal transition in ovarian cancer cells. Oncotarget. 2016;7(51):84453-67.
583 19. Ma J, Zhang J, Weng YC, Wang JC. EZH2-Mediated microRNA-139-5p Regulates Epithelial-
584 Mesenchymal Transition and Lymph Node Metastasis of Pancreatic Cancer. Mol Cells. 2018;41(9):868-
585 80.
586 20. Lachat C, Bruyere D, Etcheverry A, Aubry M, Mosser J, Warda W, et al. EZH2 and KDM6B
587 Expressions Are Associated with Specific Epigenetic Signatures during EMT in Non Small Cell Lung
588 Carcinomas. Cancers (Basel). 2020;12(12).
589 21. Lu C, Han HD, Mangala LS, Ali-Fehmi R, Newton CS, Ozbun L, et al. Regulation of tumor
590 angiogenesis by EZH2. Cancer Cell. 2010;18(2):185-97.
591 22. Liu X, Lu X, Zhen F, Jin S, Yu T, Zhu Q, et al. LINC00665 Induces Acquired Resistance to Gefitinib
592 through Recruiting EZH2 and Activating PI3K/AKT Pathway in NSCLC. Mol Ther Nucleic Acids.
593 2019;16:155-61.
594 23. Passaro A, Janne PA, Mok T, Peters S. Overcoming therapy resistance in EGFR-mutant lung
595 cancer. Nat Cancer. 2021;2(4):377-91.

596 24. Gong H, Li Y, Yuan Y, Li W, Zhang H, Zhang Z, et al. EZH2 inhibitors reverse resistance to gefitinib
597 in primary EGFR wild-type lung cancer cells. BMC Cancer. 2020;20(1):1189.
598 25. Duan R, Du W, Guo W. EZH2: a novel target for cancer treatment. J Hematol Oncol.
599 2020;13(1):104.
600 26. Pennell NA, Arcila ME, Gandara DR, West H. Biomarker Testing for Patients With Advanced
601 Non-Small Cell Lung Cancer: Real-World Issues and Tough Choices. Am Soc Clin Oncol Educ Book.
602 2019;39:531-42.
603 27. Leighl NB, Page RD, Raymond VM, Daniel DB, Divers SG, Reckamp KL, et al. Clinical Utility of
604 Comprehensive Cell-free DNA Analysis to Identify Genomic Biomarkers in Patients with Newly
605 Diagnosed Metastatic Non-small Cell Lung Cancer. Clin Cancer Res. 2019;25(15):4691-700.
606 28. Mack PC, Banks KC, Espenschied CR, Burich RA, Zill OA, Lee CE, et al. Spectrum of driver
607 mutations and clinical impact of circulating tumor DNA analysis in non-small cell lung cancer: Analysis
608 of over 8000 cases. Cancer. 2020;126(14):3219-28.
609 29. Cui W, Milner-Watts C, McVeigh TP, Minchom A, Bholse J, Davidson M, et al. A pilot of Blood-
610 First diagnostic cell free DNA (cfDNA) next generation sequencing (NGS) in patients with suspected
611 advanced lung cancer. Lung Cancer. 2022;165:34-42.
612 30. Kuang PP, Li N, Liu Z, Sun TY, Wang SQ, Hu J, et al. Circulating Tumor DNA Analyses as a
613 Potential Marker of Recurrence and Effectiveness of Adjuvant Chemotherapy for Resected Non-Small-
614 Cell Lung Cancer. Front Oncol. 2020;10:595650.
615 31. Nagasaka M, Uddin MH, Al-Hallak MN, Rahman S, Balasubramanian S, Sukari A, et al. Liquid
616 biopsy for therapy monitoring in early-stage non-small cell lung cancer. Mol Cancer. 2021;20(1):82.
617 32. Markou AN, Londra D, Stergiopoulou D, Vamvakaris I, Potaris K, Pateras IS, et al. Preoperative
618 Mutational Analysis of Circulating Tumor Cells (CTCs) and Plasma-cfDNA Provides Complementary
619 Information for Early Prediction of Relapse: A Pilot Study in Early-Stage Non-Small Cell Lung Cancer.
620 Cancers (Basel). 2023;15(6).

621 33. Gale D, Heider K, Ruiz-Valdepenas A, Hackinger S, Perry M, Marsico G, et al. Residual ctDNA
622 after treatment predicts early relapse in patients with early-stage non-small cell lung cancer. Ann
623 Oncol. 2022;33(5):500-10.
624 34. Chaudhuri AA, Chabon JJ, Lovejoy AF, Newman AM, Stehr H, Azad TD, et al. Early Detection of
625 Molecular Residual Disease in Localized Lung Cancer by Circulating Tumor DNA Profiling. Cancer Discov.
626 2017;7(12):1394-403.
627 35. Gong Y, Wei C, Cheng L, Ma F, Lu S, Peng Q, et al. Tracking the Dynamic Histone Methylation
628 of H3K27 in Live Cancer Cells. ACS Sens. 2021;6(12):4369-78.
629 36. Voigt P, Tee WW, Reinberg D. A double take on bivalent promoters. Genes Dev.
630 2013;27(12):1318-38.
631 37. Donaldson-Collier MC, Sungalee S, Zufferey M, Tavernari D, Katanayeva N, Battistello E, et al.
632 EZH2 oncogenic mutations drive epigenetic, transcriptional, and structural changes within chromatin
633 domains. Nat Genet. 2019;51(3):517-28.
634 38. Cai MY, Tong ZT, Zhu W, Wen ZZ, Rao HL, Kong LL, et al. H3K27me3 protein is a promising
635 predictive biomarker of patients' survival and chemoradioresistance in human nasopharyngeal
636 carcinoma. Mol Med. 2011;17(11-12):1137-45.
637 39. Haragan A, Field JK, Davies MPA, Escriu C, Gruver A, Gosney JR. Heterogeneity of PD-L1
638 expression in non-small cell lung cancer: Implications for specimen sampling in predicting treatment
639 response. Lung Cancer. 2019;134:79-84.
640 40. Tsai CC, Chien MN, Chang YC, Lee JJ, Dai SH, Cheng SP. Overexpression of Histone H3 Lysine 27
641 Trimethylation Is Associated with Aggressiveness and Dedifferentiation of Thyroid Cancer. Endocr
642 Pathol. 2019;30(4):305-11.
643 41. Hoffmann F, Niebel D, Aymans P, Ferring-Schmitt S, Dietrich D, Landsberg J. H3K27me3 and
644 EZH2 expression in melanoma: relevance for melanoma progression and response to immune
645 checkpoint blockade. Clin Epigenetics. 2020;12(1):24.

646 42. Holzel M, Bovier A, Tuting T. Plasticity of tumour and immune cells: a source of heterogeneity
647 and a cause for therapy resistance? Nat Rev Cancer. 2013;13(5):365-76.
648 43. Yuan S, Norgard RJ, Stanger BZ. Cellular Plasticity in Cancer. Cancer Discov. 2019;9(7):837-51.
649 44. Li J, Stanger BZ. How Tumor Cell Dedifferentiation Drives Immune Evasion and Resistance to
650 Immunotherapy. Cancer Res. 2020;80(19):4037-41.
651 45. Holdenrieder S, Nagel D, Schalhorn A, Heinemann V, Wilkowski R, von Pawel J, et al. Clinical
652 relevance of circulating nucleosomes in cancer. Ann N Y Acad Sci. 2008;1137:180-9.
653 46. Schwarzenbach H, Hoon DS, Pantel K. Cell-free nucleic acids as biomarkers in cancer patients.
654 Nat Rev Cancer. 2011;11(6):426-37.
655 47. McAnena P, Brown JA, Kerin MJ. Circulating Nucleosomes and Nucleosome Modifications as
656 Biomarkers in Cancer. Cancers (Basel). 2017;9(1).
657 48. Holdenrieder S, Stieber P, von Pawel J, Raith H, Nagel D, Feldmann K, et al. Circulating
658 nucleosomes predict the response to chemotherapy in patients with advanced non-small cell lung
659 cancer. Clin Cancer Res. 2004;10(18 Pt 1):5981-7.
660 49. Barlesi F, Mazieres J, Merlio JP, Debieuvre D, Mosser J, Lena H, et al. Routine molecular
661 profiling of patients with advanced non-small-cell lung cancer: results of a 1-year nationwide
662 programme of the French Cooperative Thoracic Intergroup (IFCT). Lancet. 2016;387(10026):1415-26.
663 50. Mitsudomi T, Hamajima N, Ogawa M, Takahashi T. Prognostic significance of p53 alterations in
664 patients with non-small cell lung cancer: a meta-analysis. Clin Cancer Res. 2000;6(10):4055-63.
665 51. Gu J, Zhou Y, Huang L, Ou W, Wu J, Li S, et al. TP53 mutation is associated with a poor clinical
666 outcome for non-small cell lung cancer: Evidence from a meta-analysis. Mol Clin Oncol. 2016;5(6):705-
667 13.
668 52. Guo Y, Song J, Wang Y, Huang L, Sun L, Zhao J, et al. Concurrent Genetic Alterations and Other
669 Biomarkers Predict Treatment Efficacy of EGFR-TKIs in EGFR-Mutant Non-Small Cell Lung Cancer: A
670 Review. Front Oncol. 2020;10:610923.

671 53. Assoun S, Theou-Anton N, Nguenang M, Cazes A, Danel C, Abbar B, et al. Association of TP53
672 mutations with response and longer survival under immune checkpoint inhibitors in advanced non-
673 small-cell lung cancer. Lung Cancer. 2019;132:65-71.
674 54. Garcia J, Dusserre E, Cheynet V, Bringuier PP, Brengle-Pesce K, Wozny AS, et al. Evaluation of
675 pre-analytical conditions and comparison of the performance of several digital PCR assays for the
676 detection of major EGFR mutations in circulating DNA from non-small cell lung cancers: the CIRCAN_0
677 study. Oncotarget. 2017;8(50):87980-96.
678 55. Bieler J, Pozzorini C, Garcia J, Tuck AC, Macheret M, Willig A, et al. High-Throughput Nucleotide
679 Resolution Predictions of Assay Limitations Increase the Reliability and Concordance of Clinical Tests.
680 JCO Clin Cancer Inform. 2021;5:1085-95.
681 56. Garcia J, Gauthier A, Lescuyer G, Barthelemy D, Geiguer F, Balandier J, et al. Routine Molecular
682 Screening of Patients with Advanced Non-SmallCell Lung Cancer in Circulating Cell-Free DNA at
683 Diagnosis and During Progression Using OncoBEAM(TM) EGFR V2 and NGS Technologies. Mol Diagn
684 Ther. 2021;25(2):239-50.
685 57. Garcia J, Kamps-Hughes N, Geiguer F, Couraud S, Sarver B, Payen L, et al. Sensitivity, specificity,
686 and accuracy of a liquid biopsy approach utilizing molecular amplification pools. Sci Rep.
687 2021;11(1):10761.

688

689 **FIGURES LEGEND**

690 **Figure 1. Quantification of circulating methylated-nucleosomes in NSCLC samples at**
691 **diagnosis and in healthy samples.** The concentration of circulating H3K27Me3-, H3K36Me3-
692 , H3K9Me3- or H3K4Me2-nucleosomes were measured using chemiluminescent Nu.Q®
693 immunoassays on human K2-EDTA plasma samples from NSCLC patients at diagnosis (DI)
694 and healthy donors. **A-B.** Box plot analysis representations circulating H3K27Me3-,
695 H3K36Me3, H3K9Me3 and H3K4Me2-nucleosome levels in NSCLC samples compared to

696 healthy samples in Training (A) and validation (B) sets. Boxes represent 25th-75th percentile
697 with median. Whiskers represent 2.5th-97.5th percentile. *** and **** represent *p*-value < 0.001
698 and < 0.0001, respectively, calculated by Mann-Whitney U test . **C-D.** Receiver-operating
699 characteristic (ROC) curve analysis of circulating H3K27Me3- and H3K4Me2-nucleosomes
700 for discrimination of NSCLC at diagnosis versus healthy samples in Training (C) and validation
701 sets (D). The areas under the curve (AUC) for the targeted nucleosome markers are indicated
702 in legend. The red line indicates the theoretical random chance. The corresponding significance
703 *p*-values for circulating H3K27Me3- and H3K4Me2-nucleosomes are respectively < 0.0001
704 and 0.0021 for the training set, $p < 0.0001$ and $p = 0.0063$ for the validation set.

705

706 **Figure 2. Correlation between methylated-nucleosome levels, cfDNA concentration and**
707 **MAF percent in global NSCLC cohort at diagnosis.** MAF % was given by SOPHIA DDM™
708 bio-informatics analysis and corresponds to ratio of the absolute count of read between mutated
709 forms on reference forms at each genomic position. Spearman's rank correlation coefficient
710 (Spearman's rho) was calculated for combinations represented in table. *** and **** represent
711 *p*-value < 0.001 and < 0.0001, respectively. The number of samples involved are indicated (n
712 =) for every correlation. Spearman's correlation coefficient ranges from 0 to 1 is represented
713 on the right panel as a color map.

714

715 **Figure 3. Representative H3K27Me3 immunostaining (10x objective). (A)** representative
716 image of normal lung tissue. **(B-D)** Representative images of weak (B), moderate (C) and high
717 (D) intensity immunostaining from lung adenocarcinoma. **(E)** H3K27Me3 expression in
718 function of grade.

719

720 **Figure 4. Quantification of circulating H3K27Me3-nucleosomes in NSCLC at diagnosis**
721 **and in healthy samples in whole cohorts. (A)** Healthy samples (black) and NSCLC samples
722 at diagnosis (DI) (white). **(B)** Healthy samples (black), NSCLC samples at DI in which somatic
723 mutation was detected (ctDNA+; dot filled) or not (ctDNA-; white), according to the somatic
724 molecular profile obtained with a panel of 78 genes containing the major oncodrivers known
725 and in NSCLC samples at DI with mutated ctDNA detected. The boxes represent 25th-75th
726 percentile with median. Whiskers represent 2.5^{th}-97.5^{th} percentile. *** and **** represent *p*-
727 value < 0.001 and < 0.0001, calculated by Mann-Whitney (groups of interest (k) = 2) and
728 Kruskal-Wallis (*k*>2) tests.

729

730 **Figure 5. Decision tree proposed for the classification of NSCLC samples at Diagnosis.**
731 The decision is based on presence/absence of circulating tumor DNA (ctDNA) and on
732 H3K27Me3-nucleosome levels below or above 22.5 ng/mL determined on K2-EDTA plasma
733 samples from NSCLC patients at diagnosis. Number of samples (n =) are presented for the
734 training (T; n = 203), the validation (V; n = 115) and the whole cohort (V+T; n = 318).
735 Percentages express the part of the total cohort involved.

736

737 **Figure 6. Quantification of circulating H3K27Me3-nucleosomes in NSCLC and healthy**
738 **samples in the whole cohort during treatment.** The concentration of circulating H3K27Me3-
739 nucleosomes was measured using chemiluminescent Nu.Q® immunoassays on human K2-
740 EDTA plasma samples from NSCLC patients during treatment (Tt) and from healthy donors.
741 **A-B.** The box plot analyses representing circulating H3K27Me3-nucleosome levels **(A)** in
742 NSCLC during treatment (white) compared with healthy samples (black). **(B)** or in NSCLC
743 samples during treatment in which mutation is detected (ctDNA+; dot filled) or not (ctDNA-;

744 white), according to the somatic molecular profile obtained with a panel of 78 genes containing
745 the major oncodrivers known in NSCLC. The boxes represent 25th-75th percentile with median.
746 Whiskers represent 2.5th-97.5th percentile. *** and **** represent *p*-value < 0.001 and <
747 0.0001, calculated by Mann-Whitney (groups of interest (k) = 2) and Kruskal-Wallis (*k*>2) tests.
748 **C.** Receiver-operating characteristic (ROC) curve analysis of circulating H3K27Me3-
749 nucleosomes. Discrimination of NSCLC during treatment versus healthy groups (grey line) is
750 compared to discrimination of NSCLC ctDNA+ during treatment versus healthy groups (black
751 line) and to discrimination of NSCLC ctDNA- during treatment versus healthy groups (dotted
752 line). The red line indicates the theoretical random chance. **D.** The groups size, areas under the
753 curve (AUC) and corresponding *p*-values for the targeted groups are listed. All analyses are
754 highly significant.

755

756 **Figure 7. Decision tree proposed for the classification of NSCLC samples during patient**
757 **follow-up. A.** The decision is based on H3K27Me3-nucleosomes levels below or above 22.5
758 ng/mL and in presence/absence of circulating tumor DNA (ctDNA) determined on K2-EDTA
759 plasma samples from NSCLC patients during treatment. Number of samples (n =) are presented
760 for the whole cohort (W; n = 304). Percentages express the part of the total cohort involved. **B.**
761 Biological and clinical interests are based on our proper interpretation and should be validated
762 clinically.

763

764 **Figure 8. H3K27Me3-nucleosome levels of NSCLC samples during treatment according**
765 **to the somatic alteration status.** The concentration of circulating H3K27Me3-nucleosomes
766 was measured using chemiluminescent Nu.Q® immunoassays on human EDTA plasma
767 samples. Only ctDNA+ group was included in this analysis. Minus (-) groups referred to

768 samples where a mutation in an oncodriver is different from the gene of interest (*EGFR*, *KRAS*
769 or *TP53*); plus (+) groups referred to samples for which at least one mutation is detected in the
770 gene of interest (*EGFR*, *KRAS* or *TP53*). **A.** Boxes represent 25th-75th percentile with median.
771 Whiskers represent 2.5^{th}-97.5^{th} percentile. * represent *p*-value < 0.05 calculated by Mann-
772 Whitney U test for testing the hypotheses of equality or difference between the two groups of
773 interest. **B**. Groups size (n =) means and medians are summarized in table.

774

775 **ADDITIONAL FILES**

776 **Fig. S1. A-B. ROC curve analyses of circulating H3K36Me3- and H3K9Me3-nucleosomes for**
777 **discrimination of NSCLC versus healthy groups.** The areas under the curve (AUC) for the targeted
778 nucleosome markers are indicated in legend. The red line indicates the theoretical random chance. All
779 curves were highly significantly different from the chance for circulating H3K36Me3- and H3K9Me3-
780 nucleosomes and the *p*-value were all < 0.0001 for the training and validation sets.

781 Additional Figures.docx

782

783 **Fig. S2. Frequencies distribution of H3K27Me3-nucleosome levels of healthy samples in training**
784 **and validation sets.** Training and validation sets are represented in white and grey bars, respectively. *y*
785 axis represents the relative frequency of samples expressed in percent of the total cohort along the
786 concentration of H3K27Me3 expressed in ng/mL on the *x* axis.

787 Additional Figures.docx

788

789 **Table S1. Fold change between levels of methylated-nucleosomes in NSCLC at diagnosis**
790 **compared to healthy samples.** The fold change represents a ratio which is computed as the median
791 level of specific circulating nucleosomes measured on NSCLC samples divided by the median level of
792 the reference Healthy samples.

Table S1.xlsx

Table S2. A-B. Sensitivity and specificity data for the ROC curves in Figure 1 and 6. Data corresponding to Figures 1 C and S1. A are presented in table S2 A (Training set); data corresponding to Figures D and S1. B are presented in table S2 B (Validation set).

Table S2.xlsx

Table S3. Sensitivity and specificity data for the ROC curve in Figure 6C.

Table S3.xlsx

Fig. 1

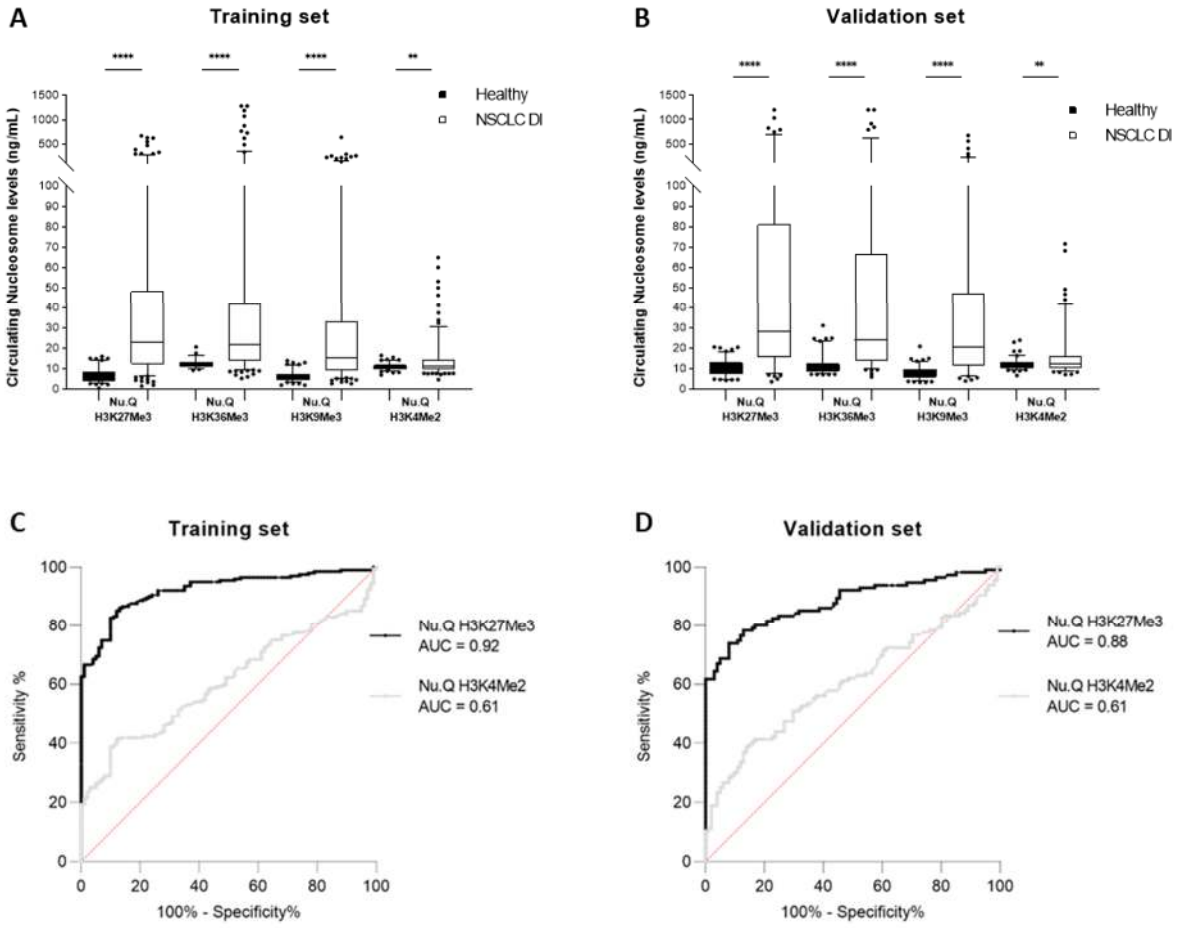
A
Training set
B
Validation set
Circulating Nucleosome levels (ng/mL)
Healthy
NSCLC DI
Nu.Q H3K27Me3
Nu.Q H3K36Me3
Nu.Q H3K9Me3
Nu.Q H3K4Me2
C
Training set
D
Validation set
Sensitivity %
100% - Specificity%
Nu.Q H3K27Me3 AUC = 0.92
Nu.Q H3K4Me2 AUC = 0.61
Nu.Q H3K27Me3 AUC = 0.88
Nu.Q H3K4Me2 AUC = 0.61

Fig. 2

Spearman's *rho*	cfDNA	MAF
H3K27me3	0,784 **** n=311	0,330 **** n=315
H3K36me3	0,661 **** n=312	0,310 **** n=316
H3K9me3	0,747 **** n=312	0,322 **** n=316
H3K4me2	0,527 **** n=305	0,214 **** n=309
cfDNA	/	0,284 *** n=309

Sig. (2-tailed) *p*-value : ***: $p < 0.001$; ****: $p < 0.0001$

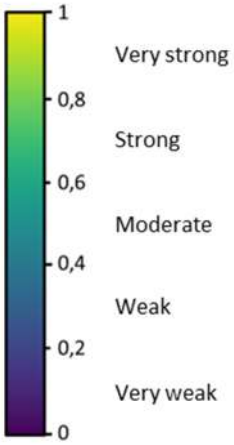

Fig. 3

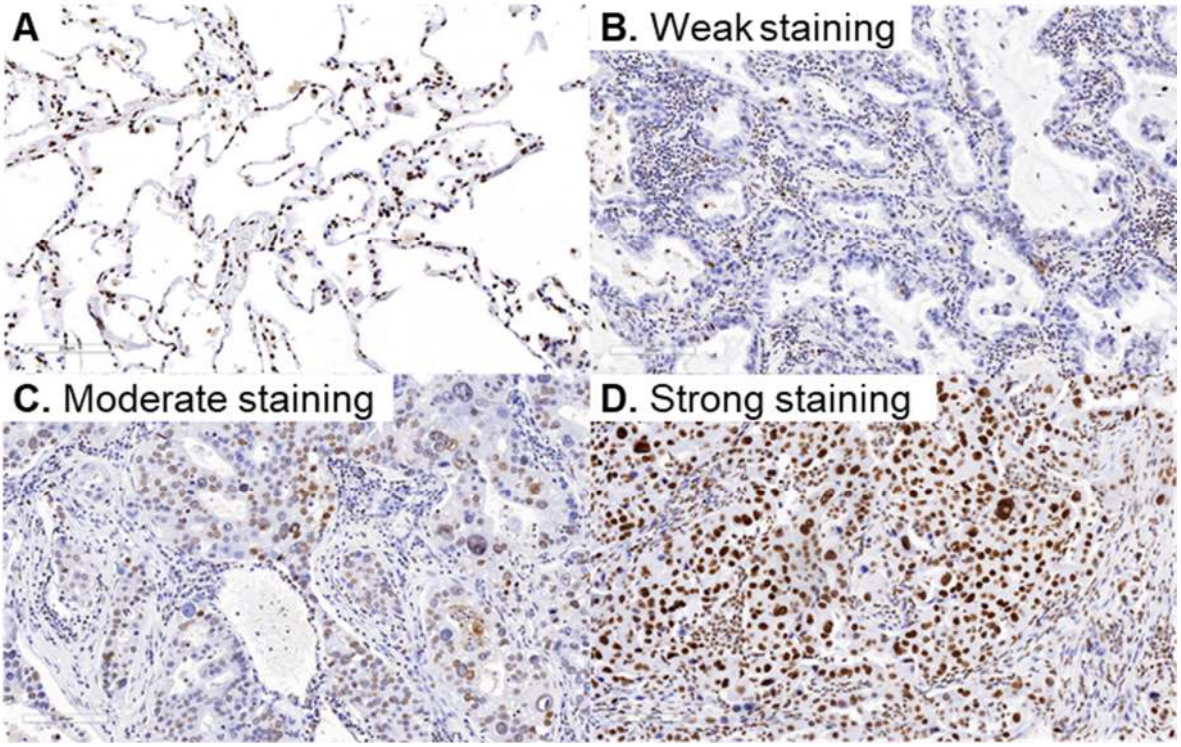
A
B. Weak staining
C. Moderate staining
D. Strong staining

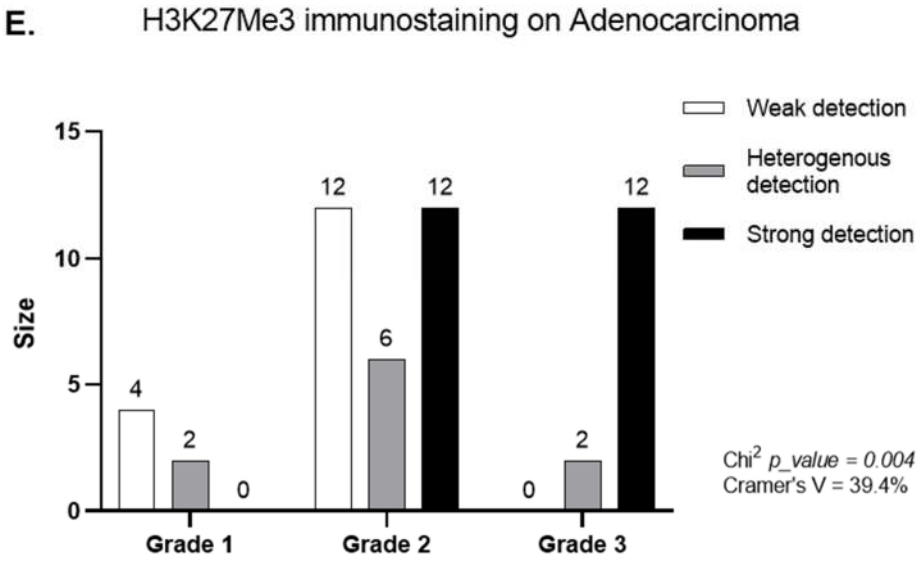
E.
H3K27Me3 immunostaining on Adenocarcinoma
Weak detection
Heterogenous detection
Strong detection
Size
15
10
5
0
4
2
0
12
6
12
0
2
12
Grade 1
Grade 2
Grade 3
Chi² p_value = 0.004
Cramer's V = 39.4%

Fig. 4

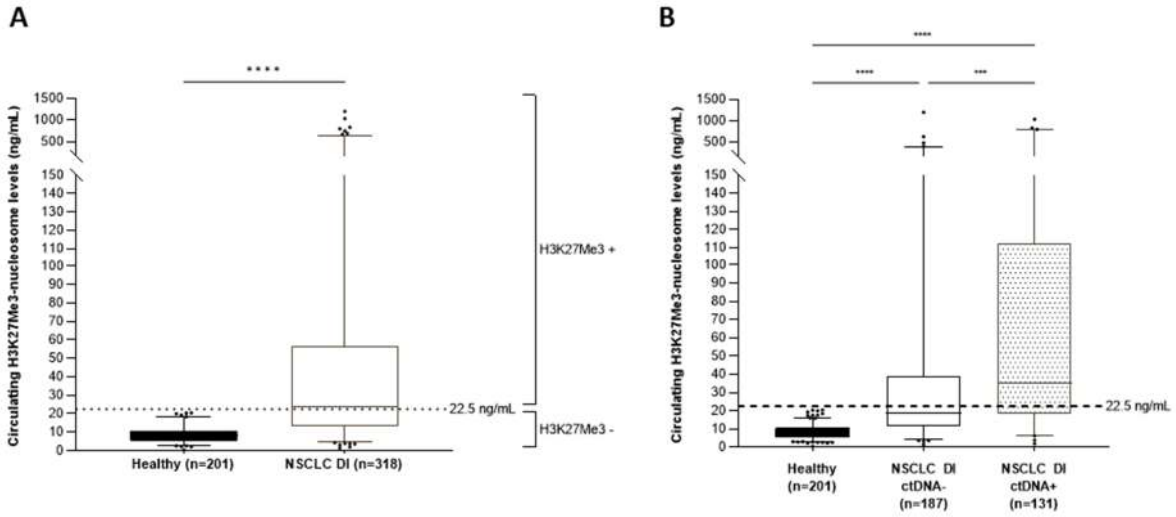
A
****
Circulating H3K27Me3-nucleosome levels (ng/mL)
1500
1000
500
150
140
130
120
110
100
90
80
70
60
50
40
30
20
10
0
22.5 ng/mL
H3K27Me3 +
H3K27Me3 -
Healthy (n=201)
NSCLC DI (n=318)
B
****
****
***
Circulating H3K27Me3-nucleosome levels (ng/mL)
22.5 ng/mL
Healthy (n=201)
NSCLC DI ctDNA- (n=187)
NSCLC DI ctDNA+ (n=131)

Fig. 5

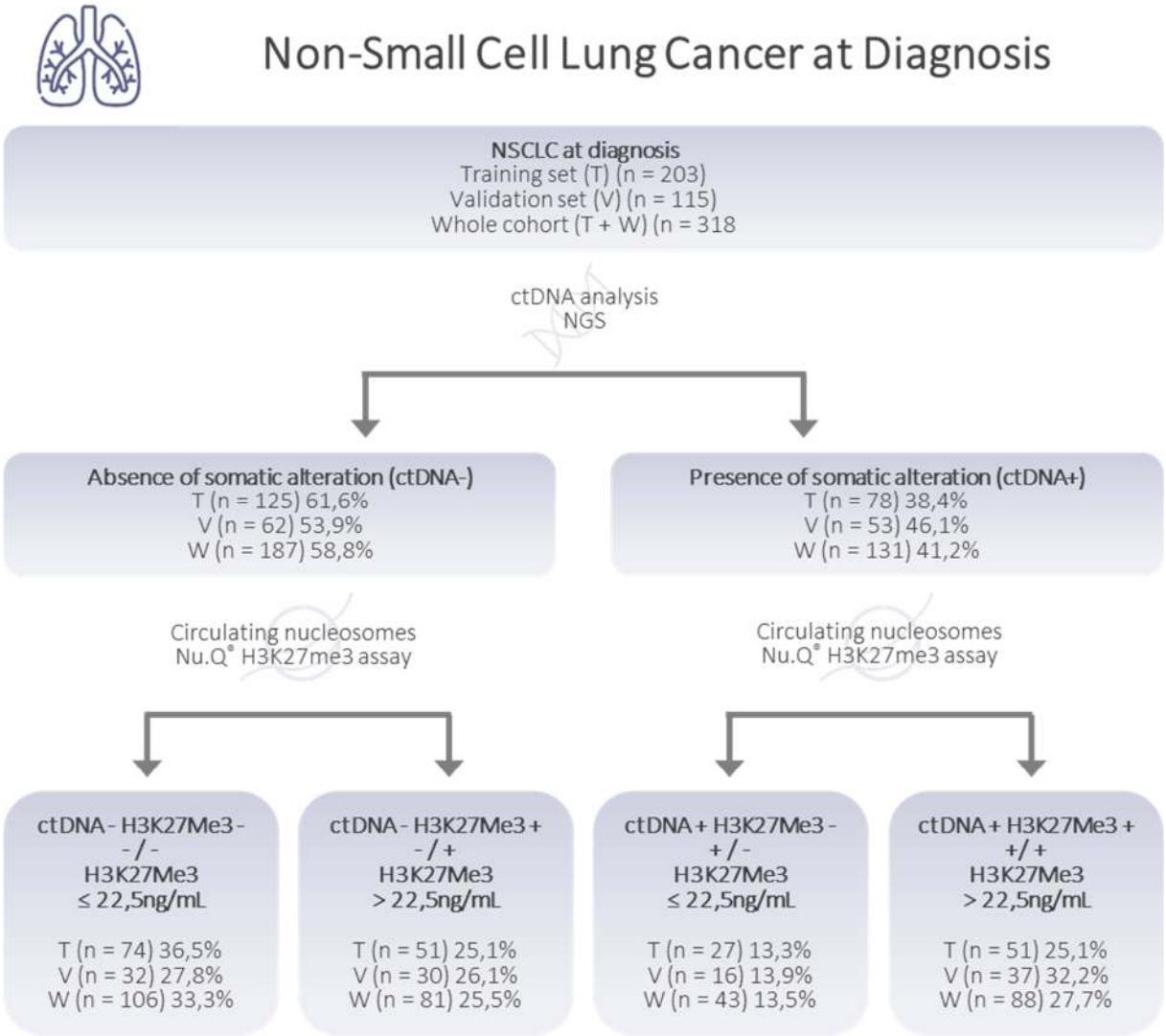
Non-Small Cell Lung Cancer at Diagnosis
NSCLC at diagnosis
Training set (T) (n = 203)
Validation set (V) (n = 115)
Whole cohort (T + W) (n = 318
ctDNA analysis
NGS
Absence of somatic alteration (ctDNA-)
T (n = 125) 61,6%
V (n = 62) 53,9%
W (n = 187) 58,8%
Presence of somatic alteration (ctDNA+)
T (n = 78) 38,4%
V (n = 53) 46,1%
W (n = 131) 41,2%
Circulating nucleosomes
Nu.Q® H3K27me3 assay
Circulating nucleosomes
Nu.Q® H3K27me3 assay
ctDNA - H3K27Me3 - - / - H3K27Me3 ≤ 22,5ng/mL
T (n = 74) 36,5%
V (n = 32) 27,8%
W (n = 106) 33,3%
ctDNA - H3K27Me3 + - / + H3K27Me3 > 22,5ng/mL
T (n = 51) 25,1%
V (n = 30) 26,1%
W (n = 81) 25,5%
ctDNA + H3K27Me3 - + / - H3K27Me3 ≤ 22,5ng/mL
T (n = 27) 13,3%
V (n = 16) 13,9%
W (n = 43) 13,5%
ctDNA + H3K27Me3 + +/ + H3K27Me3 > 22,5ng/mL
T (n = 51) 25,1%
V (n = 37) 32,2%
W (n = 88) 27,7%

Fig. 6

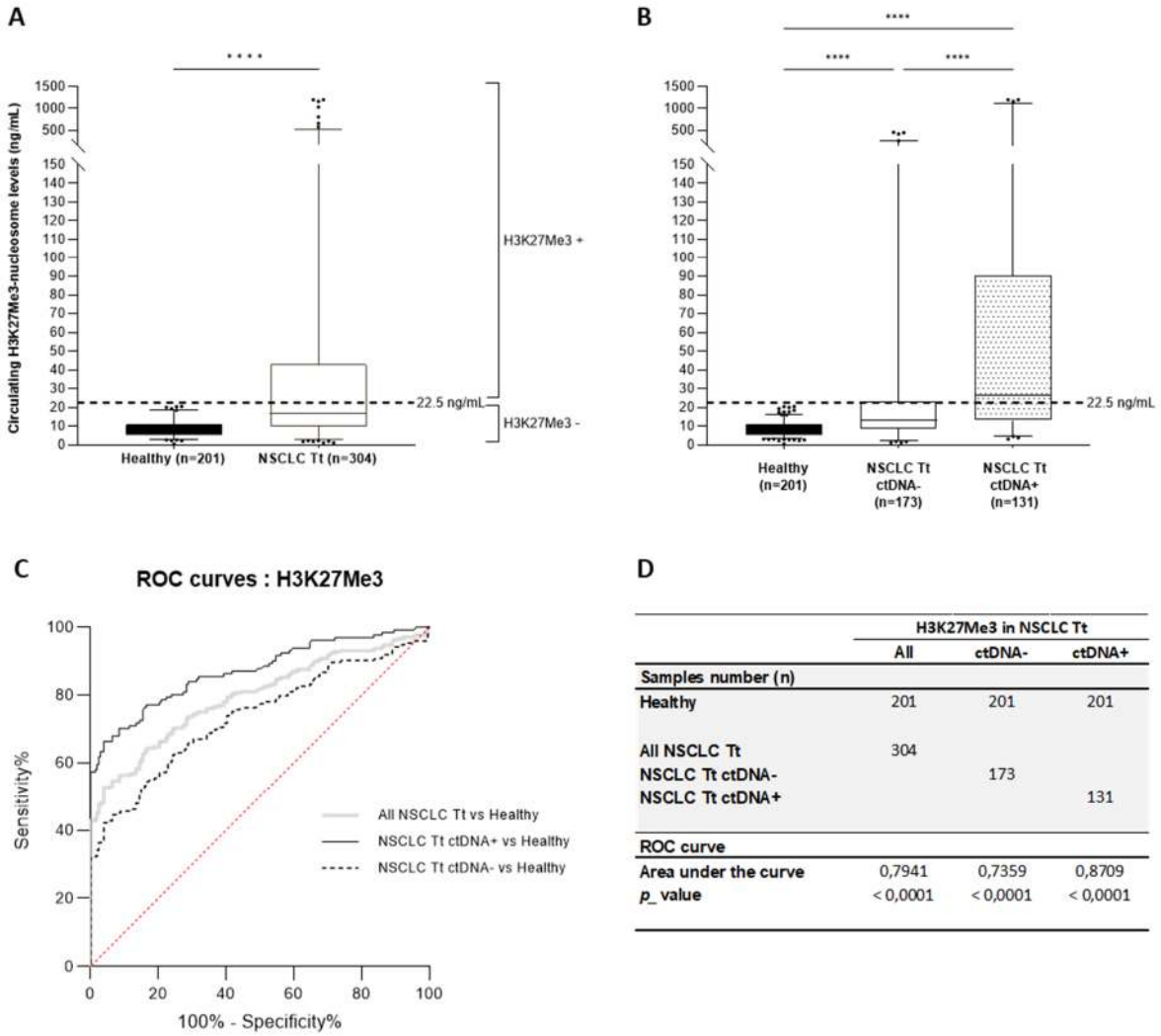

	H3K27Me3 in NSCLC Tt		
	All	ctDNA-	ctDNA+
Samples number (n)			
Healthy	201	201	201
All NSCLC Tt	304		
NSCLC Tt ctDNA-		173	
NSCLC Tt ctDNA+			131
ROC curve			
Area under the curve	0,7941	0,7359	0,8709
***p*_ value**	< 0,0001	< 0,0001	< 0,0001

Fig. 7

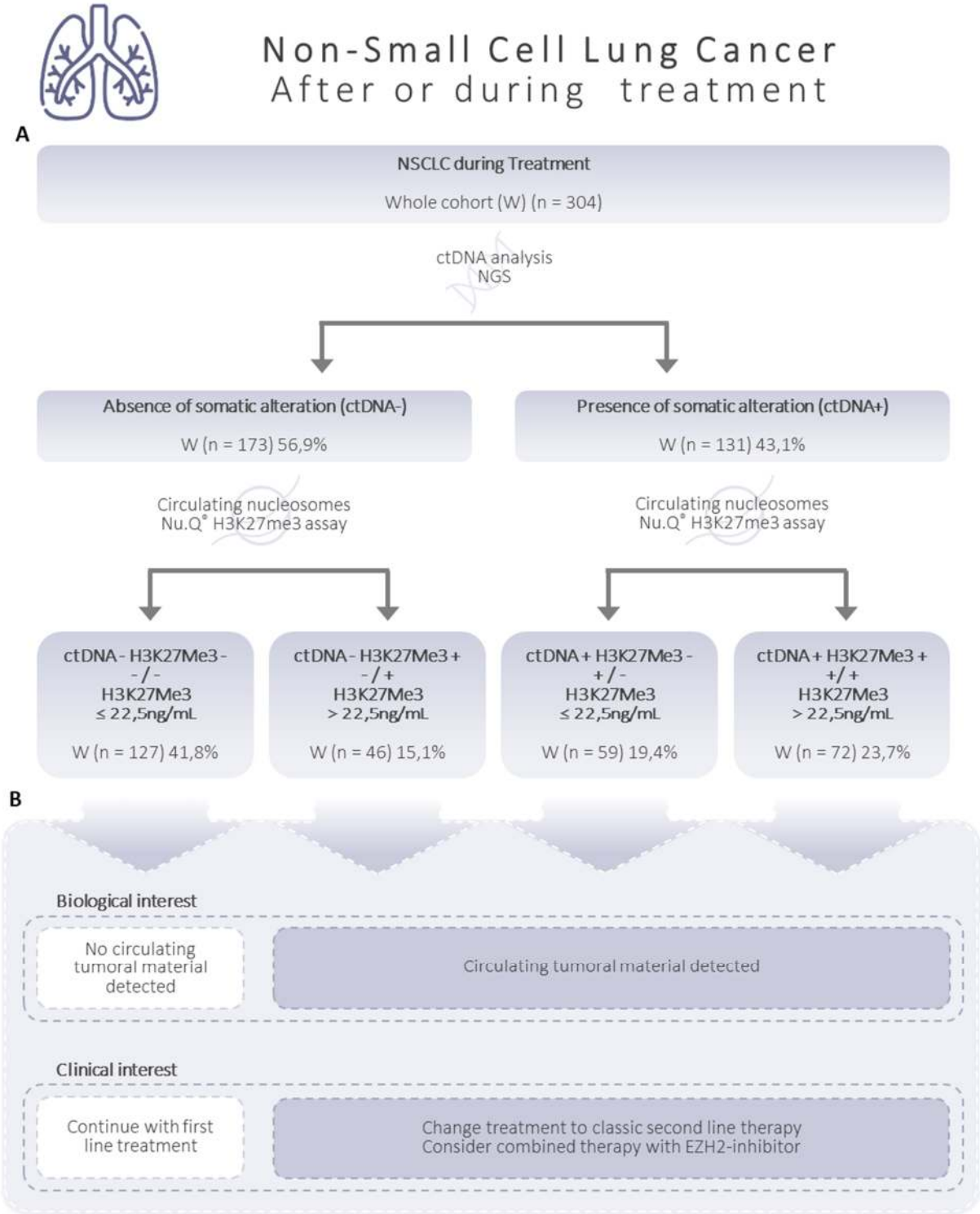
Non-Small Cell Lung Cancer
After or during treatment
A
NSCLC during Treatment
Whole cohort (W) (n = 304)
ctDNA analysis
NGS
Absence of somatic alteration (ctDNA-)
W (n = 173) 56,9%
Presence of somatic alteration (ctDNA+)
W (n = 131) 43,1%
Circulating nucleosomes
Nu.Q® H3K27me3 assay
Circulating nucleosomes
Nu.Q® H3K27me3 assay
ctDNA - H3K27Me3 - - / - H3K27Me3 ≤ 22,5ng/mL
W (n = 127) 41,8%
ctDNA - H3K27Me3 + - / + H3K27Me3 > 22,5ng/mL
W (n = 46) 15,1%
ctDNA + H3K27Me3 - + / - H3K27Me3 ≤ 22,5ng/mL
W (n = 59) 19,4%
ctDNA + H3K27Me3 + +/ + H3K27Me3 > 22,5ng/mL
W (n = 72) 23,7%
B
Biological interest
No circulating tumoral material detected
Circulating tumoral material detected
Clinical interest
Continue with first line treatment
Change treatment to classic second line therapy
Consider combined therapy with EZH2-inhibitor

Fig. 8

A

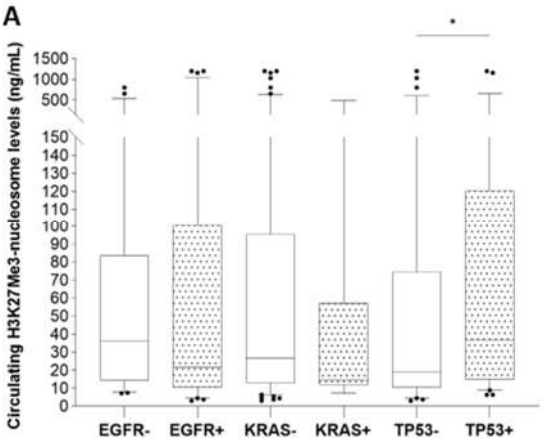

B

			H3K27me3 (ng/mL)	
		n =	mean	median
NSCLC during or after treatment		304	67,29	16,89
ctDNA-		173	31,98	13,35
ctDNA+		131	113,92	26,05
	EGFR-	53	101,91	34,08
	EGFR+	78	122,09	20,69
	KRAS-	124	115,30	26,70
	KRAS+	7	90,00	14,80
	TP53-	72	97,50	19,20
	TP53+	59	134,00	36,90